

DAMix: Density-Aware Data Augmentation for Unsupervised Domain Adaptation on Single Image Dehazing

Chia-Ming Chang¹ Chang-Sung Sung² Tsung-Nan Lin^{1,3}

¹ Graduate Institute of Communication Engineering

² Data Science Degree Program

³ Department of Electrical Engineering

National Taiwan University

{r09942090, r09946014, tsungnan}@ntu.edu.tw

Abstract

Learning-based methods have achieved great success on single image dehazing in recent years. However, these methods are often subject to performance degradation when domain shifts are confronted. Specifically, haze density gaps exist among the existing datasets, often resulting in poor performance when these methods are tested across datasets. To address this issue, we propose a density-aware data augmentation method (DAMix) that generates synthetic hazy samples according to the haze density level of the target domain. These samples are generated by combining a hazy image with its corresponding ground truth by a combination ratio sampled from a density-aware distribution. They not only comply with the atmospheric scattering model but also bridge the haze density gap between the source and target domains. DAMix ensures that the model learns from examples featuring diverse haze densities. To better utilize the various hazy samples generated by DAMix, we develop a dual-branch dehazing network involving two branches that can adaptively remove haze according to the haze density of the region. In addition, the dual-branch design enlarges the learning capacity of the entire network; hence, our network can fully utilize the DAMix-ed samples. We evaluate the effectiveness of DAMix by applying it to the existing open-source dehazing methods. The experimental results demonstrate that all methods show significant improvements after DAMix is applied. Furthermore, by combining DAMix with our model, we can achieve state-of-the-art (SOTA) performance in terms of domain adaptation.

1 Introduction

Artificial intelligence has acted as the primary driver of progress in popular fields such as computer vision. However, the degradation of information stemming from haze, fog, and smoke, often results in biases in contrast and color fidelity. In addition, contaminated images impose a burden on high-level visual tasks, such as image classification, tracking, and object detection. Therefore, image dehazing is a practical problem. One example is the single image dehazing task, which tries to recover a clean image from a single contaminated image.

To this end, traditional methods (He, Sun, and Tang 2010; Zhu, Mai, and Shao 2015; Berman, Avidan et al. 2016) rely on the atmospheric scattering model (McCartney 1976; Narasimhan and Nayar 2000, 2002), which provides a sim-

ple approximation of the haze effect by assuming that:

$$I(x) = J(x)t(x) + A(1 - t(x)), \quad (1)$$

where $I(x)$ is a hazy image composed of its corresponding haze-free image $J(x)$ and the global atmospheric light intensity A . Moreover, we have the transmission map $t(x) = e^{-\beta d(x)}$, with β and $d(x)$ being the atmospheric scattering parameter and the scene depth, respectively. To recover the haze-free image $J(x)$, these methods estimate A and $t(x)$ from the hazy image $I(x)$ by some handcrafted-priors. However, although these traditional methods work well in some cases, their strong dependency on priors may lead to poor estimation results on the transmission map when these priors do not hold. Therefore, recent research has focused on learning-based methods to avoid the need to search for robust handcrafted priors. Relying upon the strong learning capacity, these methods can directly learn the mapping from hazy to haze-free domains from existing datasets.

Nevertheless, although learning-based methods achieve state-of-the-art (SOTA) performance, they still leave plenty of room for improvement. Ideally, we can obtain a robust dehazing model as long as we have a sufficient quantity of paired data. However, collecting paired data for image dehazing is expensive and time-consuming. In addition, existing datasets are usually biased to specific environments. Consequently, the existing methods suffer from significant performance drops when confronting domain shifts in practice due to variations in position, weather conditions, and haze density. Hence, before putting these methods into actual use, they must gain the ability to transfer their learned knowledge from the source domain containing abundant paired data to the target domain containing unpaired data.

The problem mentioned above is also known as unsupervised domain adaptation, which is a learning framework that aims to learn a good estimation model for the target domain using only the paired data in the source domain. One straightforward way to address this issue is to rely on generative models such as a generative adversarial network (GAN). By generating samples that appear as if they are drawn from the target domain, learning-based methods can achieve domain adaptation by training on these samples. For instance, (Shao et al. 2020) employs CycleGAN (Zhu et al. 2017) to translate images between synthetic and real domains. By training with original and translated samples,

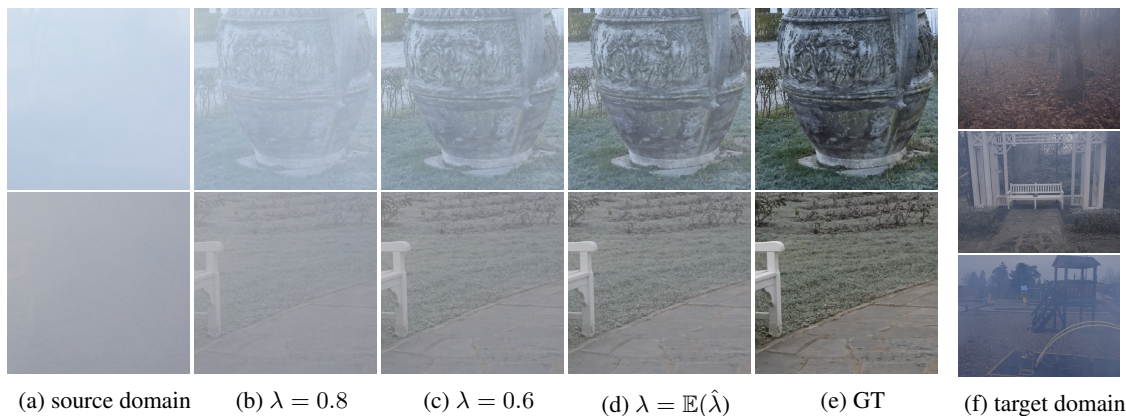


Figure 1: Samples generated from DAMix. We propose DAMix, a straightforward data augmentation method on single image dehazing. This method generates samples that bridge the haze density gap between the source domain and the target domain to address domain adaptation. (a) shows some hazy samples from the source domain (Dense-Haze), and (e) shows their corresponding ground truth. (b), (c), and (d) are samples generated from DAMix with descending λ . (f) shows a few samples from the target domain (O-Haze).

the dehazing network can achieve better results on the real domain. However, these generative models suffer from following limitations. (1) Since the existing real haze datasets consist of images covered by thick haze, it is difficult for the generative models to capture useful information from these images. Therefore, when translating the images from these kinds of datasets, these generative models often produce defective samples or artifacts. (2) Due to the black-box nature of these models, the generated samples lack interpretability. (3) Training a translation model consumes considerable amounts of time and GPU resources.

Given the above issues, we introduce a data augmentation method named density-aware data augmentation (DAMix) for domain adaptation. As shown in Fig. 1, DAMix generates a continuous sequence of synthetic hazy samples featuring haze densities ranging from that of the source domain to that of the target domain. These samples are generated by combining the hazy image with its ground truth by a sampled combination ratio. After learning from these DAMix-ed samples with various haze densities, learning-based methods can perform better when encountering domain shifts. In addition, we also propose a dual-branch network named adaptive dehazing network (ADN) to cope with domain shifts. ADN consists of a primary branch and an enhanced branch, which work with regions possessing different haze densities. Moreover, we design the density-attention loss (DAL) function to force the two branches to complement each other explicitly. In summary, our contributions offer a number of advantages over the existing methods:

Data Augmentation: We introduce a novel data augmentation method named DAMix to address domain adaptation on single image dehazing. DAMix can generate samples with an unlimited haze density mitigating the haze density gap between domains. In addition, we show that DAMix can further improve the performance of various dehazing methods when confronting domain shifts.

Density-Aware: We propose a density-aware learning

framework that explicitly forces the modules in our network to achieve division of labor. With the help of the dual-branch design and the DAL function, ADN achieves SOTA performances on several datasets. Moreover, coupled with DAMix, ADN also addresses the domain shift problem on single image dehazing with admirable results.

Interpretability: Unlike the existing methods that apply GANs to achieve style transfer, which passes the input into a black box, we show that the DAMix algorithm merely manipulates the unknown transmission map to generate hazy samples featuring diverse haze densities. We also demonstrate that DAMix-ed samples are guaranteed to comply with the atmospheric scattering model.

However, notably, DAMix can adapt only to target domains with thinner haze than the haze in the source domain. Therefore, in practice, we have to ensure that there exists sufficiently hazy images to perform DAMix to help domain adaptation. Owing to the existing datasets such as Dense-Haze (Ancuti et al. 2019a) and NH-Haze (Ancuti, Ancuti, and Timofte 2020), consisting of samples covered by thick haze, we can easily augment training samples by applying DAMix on these datasets.

2 Related Works

Single image dehazing aims to recover a haze-free image from a corresponding hazy image. The existing dehazing methods can be classified into prior-based methods and learning-based methods.

2.1 Prior-based Methods

Most prior-based methods rely on the atmospheric scattering model and employ strong priors or assumptions to restore the transmission map and the global atmospheric light intensity from the hazy image. Representative works utilizing prior-based methods include (He, Sun, and Tang 2010; Zhu, Mai, and Shao 2015; Berman, Avidan et al. 2016). (He, Sun, and Tang 2010) introduces the dark channel prior as an

additional constraint to estimate haze-free images. The dark channel prior is based on the observation that in haze-free patches, at least one of the color channels has some pixels whose intensity is very low or close to zero. (Zhu, Mai, and Shao 2015) proposes the color attenuation prior, which assumes that the scene depth is positively correlated with the difference between the brightness and the saturation. (Berman, Avidan et al. 2016) relies on the assumption that a few distinct colors can effectively represent the colors of a haze-free image. Due to the haze effect, these varying distances translate to different transmission coefficients; therefore, each color cluster in the haze-free image becomes a haze-line in RGB space. Nevertheless, although these methods show good performance under certain circumstances, their strong dependency on priors and the atmospheric scattering model may degrade the performance when confronted with complex realistic scenes not contained within the priors or the atmospheric scattering model.

2.2 Learning-based Methods

Early works follow the atmospheric scattering model by directly estimating the global atmospheric light intensity and the transmission map from the corresponding hazy image. For example, (Li et al. 2017) utilizes a simple CNN-based architecture to predict the transmission map and the global atmospheric light intensity. However, the performance of these works relies strongly on estimating the transmission map and the global atmospheric light intensity. Therefore, recent works have focused on the end-to-end prediction of haze-free images from the hazy images. (Liu et al. 2019) proposes an autoencoder endowed with a multiscale and channelwise attention mechanism. To focus more on regions with thick haze, (Qin et al. 2020) proposes a network utilizing a feature attention module that combines the channel attention and pixel attention mechanisms. (Hong et al. 2020) proposes a knowledge distillation network by learning additional information from an intermediate representation of the teacher network. (Wu et al. 2021) applies the method of contrastive learning to image dehazing by pulling the anchor (model output) close to positive points (ground-truth) and pushing the anchor far from negative points (hazy input) in the feature space. Unfortunately, although these works report admirable performance, they all suffer from significant performance drops when confronting domain shifts. Recently, several works have attempted to address this issue. (Shao et al. 2020) indicates that a model trained on synthetic hazy images cannot exhibit a sufficient generalization performance on real hazy images and therefore introduces a domain adaptation paradigm with an image translation module to bridge the gap between the synthetic and real domains. In addition, (Shyam, Yoon, and Kim 2021) applies frequency information to adversarial training with the aggregated dataset to achieve domain-invariant performance.

3 Proposed Method

We begin by describing our data augmentation method, DAMix, which does not require any training. Then we present the details regarding ADN and our DAL function.

3.1 Density-Aware Data Augmentation

Algorithm. In unsupervised domain adaptation on single image dehazing, we are given a labeled dataset $\mathbf{D}^s = \{\mathbf{I}_i^s, \mathbf{J}_i^s\}_{i=1}^{N^s}$ where \mathbf{I}^s is a hazy image sampled from the source domain, and \mathbf{J}^s is the corresponding ground-truth image. Likewise, we are also given an unlabeled dataset $\mathbf{D}^t = \{\mathbf{I}_i^t\}_{i=1}^{N^t}$ where \mathbf{I}^t is a hazy image sampled from the target domain. In most cases, learning-based models trained on \mathbf{D}^s suffer a significant performance drop when tested on \mathbf{D}^t . We therefore introduce a data augmentation method named DAMix to bridge the gap between the source domain and the target domain to address this issue.

A hazy image includes several properties, such as scene, depth, and haze density. We consider haze density the most crucial factor among these properties because we observe that haze density differs among the existing datasets. Therefore, DAMix focuses on bridging the haze density gap between the source and target domain to achieve domain adaptation. According to the color attenuation prior (Zhu, Mai, and Shao 2015), haze density is positively correlated with brightness. For simplicity, we assume that haze density can be represented by brightness. Let $\mu(\cdot) : \mathcal{R}^{H \times W \times 3} \rightarrow \mathcal{R}$ be the operation of computing the arithmetic mean. Considering the effect that context in hazy images also influences the brightness, we calculate the mean brightness of the hazy images in the target domain $\bar{\mathbf{l}}$ as the haze density. However, to maintain few variations, we sample the haze density target for domain adaptation \mathbf{L}^t as follows:

$$\mathbf{L}^t \sim \mathcal{N}(\bar{\mathbf{l}}, (\rho \times \bar{\mathbf{l}})^2), \text{ where } \bar{\mathbf{l}} = \frac{1}{N^t} \sum_{i=1}^{N^t} \mu(\mathbf{I}_i^t). \quad (2)$$

We empirically set ρ to 0.02. DAMix can then be formulated by combining a hazy image \mathbf{I}^s and its corresponding ground truth \mathbf{J}^s by the combination ratio $\lambda \in [0, 1]$ as follows:

$$\hat{\mathbf{I}}(x) = \lambda \mathbf{I}^s(x) + (1 - \lambda) \mathbf{J}^s(x). \quad (3)$$

To bridge the haze density gap between domains while maintaining the diversity, λ is sampled according to:

$$\lambda \sim [\hat{\lambda}, 1.0], \text{ where } \hat{\lambda} = \frac{\mathbf{L}^t - \mu(\mathbf{J}^s)}{\mu(\mathbf{I}^s) - \mu(\mathbf{J}^s)}. \quad (4)$$

$\hat{\lambda}$ is the density-aware ratio calculated by matching the haze density of $\hat{\mathbf{I}}$ to \mathbf{L}^t . Fig. 1 shows a few examples of DAMix. In the training phase, each training pair in the mini-batch $(\mathbf{I}^s, \mathbf{J}^s)$ is probabilistically DAMix-ed to $(\hat{\mathbf{I}}, \mathbf{J}^s)$ according to Eq. 3. Code-level details are shown in the supplementary.

Discussion. Unlike other GAN-based methods that often yield artifacts in their synthetic samples, DAMix is a robust algorithm that generates natural samples and while maintaining diversity of the haze density. Based on Eq. 1 and Eq. 3, a DAMix-ed sample can be rewritten as follows:

$$\begin{aligned} \hat{\mathbf{I}}(x) &= \lambda \mathbf{I}^s(x) + (1 - \lambda) \mathbf{J}^s(x) \\ &= \lambda(\mathbf{J}^s(x)t(x) + A(1 - t(x))) + (1 - \lambda)\mathbf{J}^s(x) \\ &= \mathbf{J}^s(x)(1 - \lambda(1 - t(x)) + A(\lambda(1 - t(x)))) \\ &= \mathbf{J}^s(x)\hat{t}(x) + A(1 - \hat{t}(x)) \end{aligned} \quad (5)$$

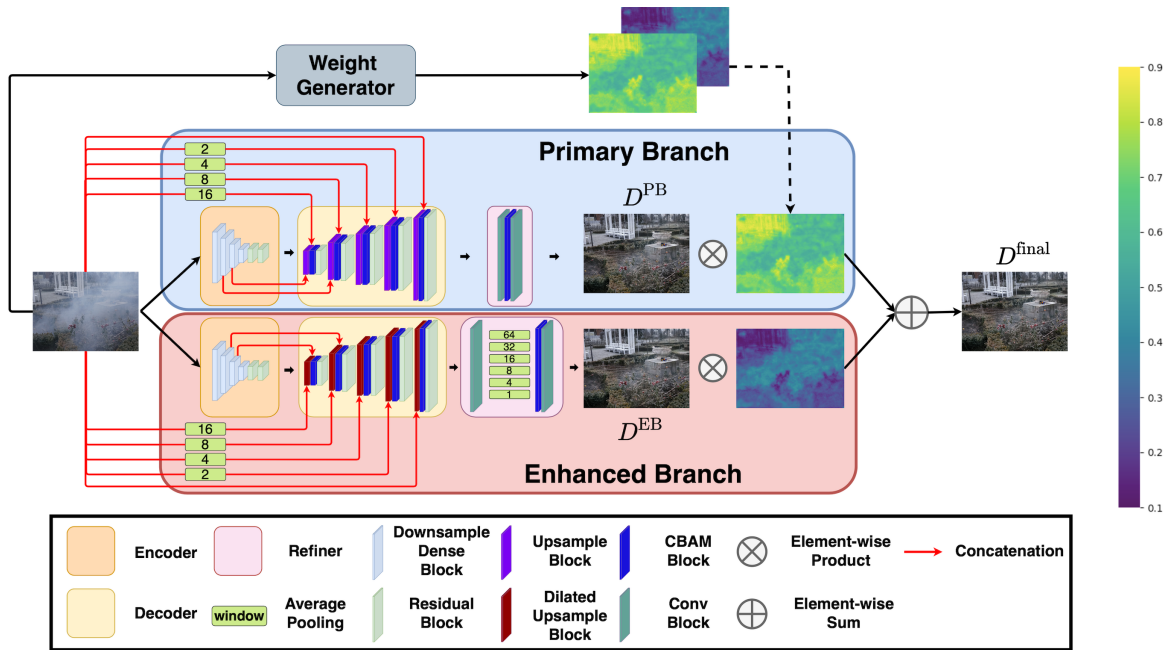


Figure 2: Overview of our Adaptive Dehazing Network.

where the DAMix-ed sample \hat{I} complies with the atmospheric scattering model with a new transmission map $\hat{t}(x) = 1 - \lambda(1 - t(x))$. Evidently, DAMix generates samples by manipulating the transmission map, and therefore DAMix-ed samples can retain their natural appearances despite the translation. Moreover, as shown in Fig. 1, DAMix generates samples featuring haze densities ranging from that of the source domain to that of the target domain. These results imply that DAMix-ed samples do bridge the gap between domains (more examples are provided in the supplementary). By learning from natural samples that bridge the haze density gap, learning-based methods can better achieve domain adaptation. Most importantly, since DAMix operates only on the data level, we can directly utilize it with any learning-based method to improve the domain adaptation performance without any computational overhead.

3.2 Adaptive Dehazing Network

To cope with hazy images exhibiting various haze density levels generated by DAMix, we propose a dual-branch dehazing network, ADN, which adaptively works with regions covered by thin or thick haze. Moreover, we introduce a DAL function weighted by the haze density to explicitly force the two branches to cooperate.

Information Flow. Let I and J denote a hazy image and its corresponding haze-free image. As shown in Fig. 2, the primary branch and the enhanced branch generate preliminary dehazed images D^{PB} and D^{EB} , respectively. To combine the preliminary outputs of the two branches, we design a weight generator, which generates two one-channel weight maps for the outputs of the two branches. Afterward, the preliminary outputs of the two branches are multiplied by their

corresponding weight maps and are then summed to obtain the final haze-free result D^{final} .

Network Architecture. As shown in Fig. 2, ADN consists of two branches, the primary branch and the enhanced branch. The primary branch manages the comprehensive removal of haze. In contrast, the enhanced branch compensates by focusing on the most severely contaminated areas that the primary branch does not thoroughly remove.

Inspired by (Zhang, Sindagi, and Patel 2018), the encoder of both branches consist of residual blocks and several dense blocks from DenseNet (Huang et al. 2017). Moreover, skip connections from the encoder and the input are employed to help the decoder better recover the structure of the haze-free image. To help the decoder pay attention to the more essential feature maps, we employ a convolutional block attention module (CBAM) block (Woo et al. 2018) in combination with spatial and channel attention after each feature concatenation. Since the enhanced branch is designed to cope with the severely contaminated regions, we apply two modifications to increase the receptive field. First, we replace the convolutional layers in the upsampling blocks with the dilated convolutional layers. Second, we adopt the pyramid pooling module in the refiner block. Similar to the pyramid scene parsing network (Zhao et al. 2017), our main idea is to fuse the hierarchical global aggregated features containing information from different scales. More details about these modules are provided in the supplementary.

Loss Function for the Primary Branch. To optimize the primary branch, we adopt the simple L1 loss:

$$\mathcal{L}^1(D, J) = \frac{1}{N} \sum_{x=1}^N |D(x) - J(x)|, \quad (6)$$

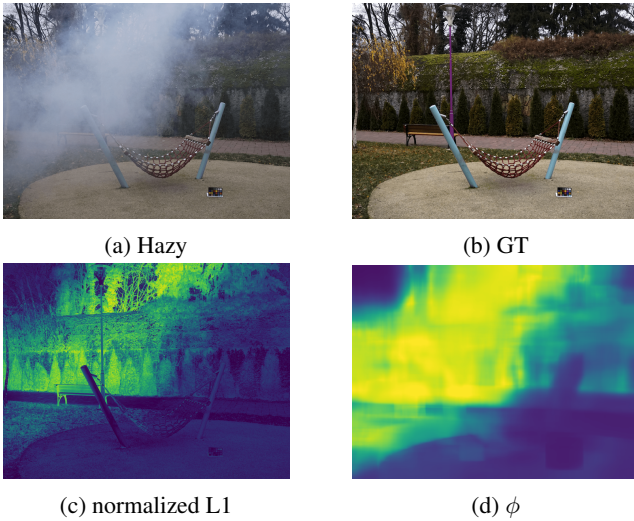


Figure 3: Visualization of haze density by using (c) normalized L1 difference and (d) ϕ as metric.

where $D(x)$ and $J(x)$ denotes the values in the dehazed image and the corresponding ground truth, respectively, at pixel x . In addition, to better preserve the contrast and the structure, we employ the multiscale structural similarity (MS-SSIM) loss. We follow the notation in (Zhao et al. 2016) and define the MS-SSIM loss as:

$$\mathcal{L}_{D,J}^{\text{MS-SSIM}}(x) = 1 - l_M^\alpha(x) \cdot \prod_{j=1}^M cs_j^{\beta_j}(x), \quad (7)$$

where l_M and cs_j are the luminance and structural similarity with scale M and j , respectively. We empirically set $\alpha = \beta_j = 1$ for $j \in \{1, \dots, M\}$, where M denotes the total number of scales. The optimization function for the primary branch \mathcal{L}^{PB} is then shown in the following:

$$\mathcal{L}^{\text{PB}} = \mathcal{L}^{\text{L1}}(D^{\text{PB}}, J) + \gamma \mathcal{L}^{\text{MS-SSIM}}(D^{\text{PB}}, J). \quad (8)$$

Loss Function for the Enhanced Branch. Since the responsibility of the enhanced branch is to remove heavy haze, we introduce the DAL function to explicitly force this branch to focus on severely contaminated regions. To better represent the haze density within an image, instead of applying a pointwise computation such as the normalized L1 difference between the hazy image I and ground-truth image J proposed by (Hong et al. 2020), we adopt the SSIM metric, which involves a patchwise computation. We formulate the haze density ϕ at pixel x as follows:

$$\phi(x) = 1 - \text{SSIM}_{I,J}(x). \quad (9)$$

As shown in Fig. 3, the haze density estimated by the SSIM metric better matches the human perception of the haze effect than that estimated by the normalized L1 difference. Therefore, we utilize ϕ to weight the L1 loss function, thereby forcing the enhanced branch to focus on areas featuring heavy haze. According to Eq. 6, the weighted L1 loss function $\mathcal{L}^{\text{w-L1}}$ can be defined as:

$$\mathcal{L}^{\text{w-L1}}(D, J) = \frac{1}{N} \sum_{x=1}^N \phi(x) \cdot |D(x) - J(x)|. \quad (10)$$

In addition, we weight the MS-SSIM loss with ϕ to force the enhanced branch to learn the structural information in regions covered by heavy haze. The DAL function can thus be formulated as follows:

$$\mathcal{L}^{\text{DAL}} = \mathcal{L}^{\text{w-L1}}(D^{\text{EB}}, J) + \gamma \mathcal{L}^{\text{w-MS-SSIM}}(D^{\text{EB}}, J). \quad (11)$$

Loss Function for the Weight Generator. To optimize the weight generator, we follow the loss function in Eq. 8 to comprehensively remove haze, which is defined as:

$$\mathcal{L}^{\text{WG}} = \mathcal{L}^{\text{L1}}(D^{\text{final}}, J) + \gamma \mathcal{L}^{\text{MS-SSIM}}(D^{\text{final}}, J). \quad (12)$$

It is worth noting that these three modules are optimized with unique objective functions. In other words, they are optimized individually in the training phase.

4 Experiments

4.1 Datasets and Evaluation Metrics

To evaluate the domain adaptation performance, we select datasets with different haze densities and distributions: Dense-Haze (Ancuti et al. 2019a), NH-Haze (Ancuti, Ancuti, and Timofte 2020), O-Haze (Ancuti et al. 2018), and SOTS-Out (Li et al. 2018). Furthermore, three real-world datasets, namely, O-Haze, NH-Haze and Dense-Haze, are adopted to evaluate the performance of ADN within the training distribution. The properties of these datasets are provided in the supplementary. To compare the performance among different methods, we utilize PSNR and SSIM as evaluation metrics, as they are often used to evaluate image quality in image restoration tasks.

4.2 Experiments on Domain Adaptation

We evaluate the effectiveness and robustness of DAMix by applying it to recent open-source learning-based methods (GridDehazeNet (Liu et al. 2019), FFA-Net (Qin et al. 2020), MSBDN (Dong et al. 2020)) and ADN. Since DAMix can adapt only to a domain with thinner haze, we sort the four datasets according to the haze density in descending order: Dense-Haze, NH-Haze, O-Haze, and SOTS-Out. Then, we conduct several domain adaptation experiments following the haze density order mentioned above.

As shown in Tab. 1, all the models notably improve with respect to almost all settings when DAMix is applied in the training phase. As the difference in the haze density between the source and target domains increases, models trained with DAMix show greater improvement in terms of PSNR/SSIM. Especially in the Dense-Haze \rightarrow SOTS-Out setting, DAMix achieves average performance gains equaling a PSNR of 5.80 dB, and an SSIM of 0.1702 over the four models. As shown in Fig. 4, the models trained without DAMix suffer from a color shift and overenhancement in the sky and the buildings (see the supplementary for more examples). With the help of DAMix, these models can recover more precise and realistic colors. These synthetic samples not only comply with the atmospheric scattering model but also provide models with more diversity of the haze density. In addition, ADN trained with DAMix achieves either the best or second best performance in each setting. We attribute this result to the dual-branch design in ADN, which enlarges the

Source Domain		Dense-Haze			NH-Haze		O-Haze
Target Domain		NH-Haze	O-Haze	SOTS-Out	O-Haze	SOTS-Out	SOTS-Out
GridDehazeNet (ICCV'19)	w/o DAMix	15.78/0.593	16.11/0.579	13.27/0.615	18.38/0.629	14.35/0.738	18.96/0.815
	with DAMix	15.82/0.604	19.84/0.685	18.27/ <u>0.808</u>	18.61/0.657	15.63/0.779	20.12/0.838
FFA-Net (AAAI'20)	w/o DAMix	17.10/0.629	18.93/0.640	16.61/0.704	19.17/0.643	16.69/0.785	<u>20.64</u> / 0.850
	with DAMix	17.07/ <u>0.634</u>	19.13/0.618	19.87/0.779	19.59/0.675	<u>17.81</u> / <u>0.806</u>	20.40/ <u>0.849</u>
MSBDN (CVPR'20)	w/o DAMix	15.87/0.595	18.39/0.673	12.95/0.631	18.73/0.649	14.12/0.719	18.78/0.797
	with DAMix	15.47/0.600	<u>21.54</u> / <u>0.694</u>	21.92 / 0.858	19.74/0.662	16.43/0.790	19.61/0.812
ADN (Ours)	w/o DAMix	<u>18.03</u> /0.629	20.51/0.690	15.04/0.672	<u>19.89</u> / <u>0.685</u>	15.90/0.756	19.80/0.819
	with DAMix	18.20 / 0.649	21.73 / 0.739	<u>21.01</u> / 0.858	21.28 / 0.736	18.93 / 0.826	21.41 /0.830

Table 1: Quantitative improvements in the domain adaptation performance by applying DAMix. We adopt the **PSNR/SSIM** as evaluation metrics. **Boldface** and underlined values indicate the best and second best result, respectively, for each setting.

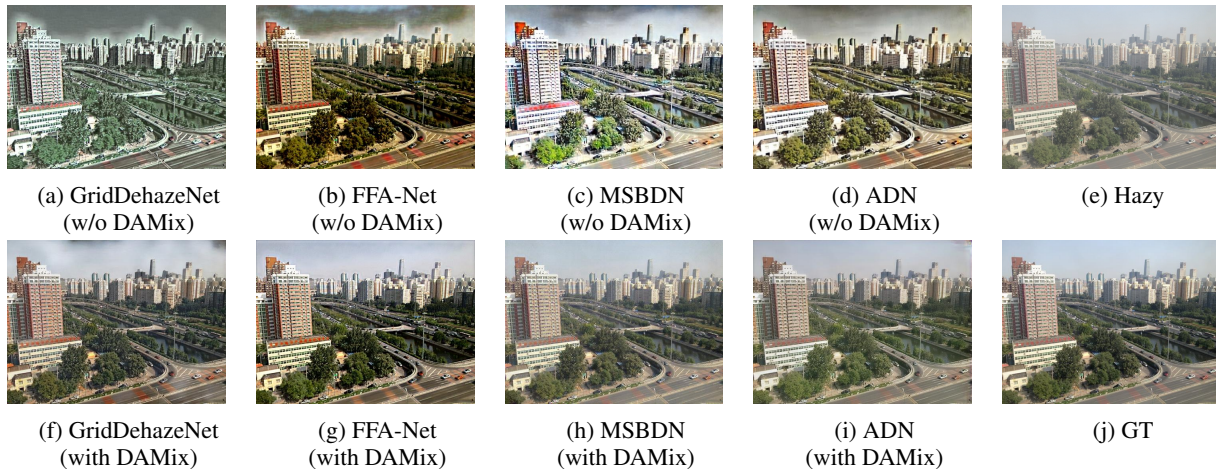


Figure 4: Qualitative results of the models trained on Dense-Haze and tested on SOTS-Out.

learning capacity of the entire framework. Owing to DAMix, which provides diverse and natural training samples, ADN can achieve admirable performance on domain adaptation, indicating that the combination of DAMix with ADN is superior to other options for domain adaptation.

4.3 Comparison with Other Data Augmentation

We compare DAMix with the greedy localized data augmentation (GLDA) algorithm proposed by (Shyam, Yoon, and Kim 2021). GLDA aims to generate samples with a nonhomogeneous haze distribution. Therefore, we conduct experiments under the Dense-Haze→NH-Haze setting. As

shown in Tab. 2, DAMix outperforms GLDA except on MSBDN. In particular, DAMix with ADN achieves notable improvements (0.17 dB in PSNR and 0.020 in SSIM) compared with those of GLDA. We attribute this result to the discontinuous hazy samples generated by GLDA (examples are shown in the supplementary). In contrast, DAMix generates smoother hazy samples that are more natural from a human perspective. In addition to GLDA, we utilize CycleGAN of (Shao et al. 2020) to perform data augmentation. However, the generated samples are flawed in comparison with those produced by DAMix and GLDA; this is probably due to the severely contaminated samples within the exist-

ing real-world haze datasets, as it is difficult for this kind of unsupervised generative model to generate satisfactory samples.

Method	w/o Aug.	GLDA	DAMix
GridDehazeNet	15.78/0.593	15.79/0.537	15.82/0.604
FFA-Net	17.10/0.629	15.84/0.561	17.07/ 0.634
MSBDN	15.87/0.595	16.16/0.588	15.47/ 0.600
ADN (Ours)	18.03/0.629	18.03/0.637	18.20/0.649

Table 2: Comparison with GLDA.

4.4 Experiments within the Training Distribution

To evaluate the ability of ADN to remove haze from samples within the training distribution, we compare ADN with the SOTA methods (DCP (He, Sun, and Tang 2010), AOD-Net (Li et al. 2017), GridDehazeNet (Liu et al. 2019), FFA-Net (Qin et al. 2020), MSBDN (Dong et al. 2020), KDDN (Hong et al. 2020), AECR-Net (Wu et al. 2021)) on O-Haze (Ancuti et al. 2018), Dense-Haze (Ancuti et al. 2019a), and NH-Haze (Ancuti, Ancuti, and Timofte 2020) datasets. We follow the setting of the NTIRE Image Dehazing Challenges (Ancuti, Ancuti, and Timofte 2018; Ancuti et al. 2019b, 2020) to evaluate these methods. For the open-source methods, we stick to their respective methods and retrain on the above-mentioned datasets if the results of any of these datasets are not reported in their papers. As shown in Tab. 3, ADN outperforms all SOTA methods on the above three datasets. Specifically, we observe that: (1) ADN surpasses the second best SSIM with 0.076 on the Dense-Haze dataset and (2) ADN achieves the highest PSNR of 21.03 dB on the NH-Haze dataset, surpassing by 1.15 dB that of AECR-Net, whose SSIM is only 0.003 lower. These two datasets consist of hazy samples covered by real dense haze, which is difficult to remove. Existing methods often fail to recover either the structural information or the color fidelity from regions covered by dense haze. However, due to the dual-branch design and CBAM attention module, ADN can better recover the color fidelity and structural details. Qualitative examples are given in the supplementary.

4.5 Ablation Study

Next, we conduct an ablation study to examine the effects of the modules in ADN. We construct five settings as follows: (1) **PB**: Using the primary branch but not the CBAM. (2) **PB+EB**: Using the primary branch and the enhanced branch but not the CBAM. (3) **PB+CBAM**: Using the primary branch with the CBAM. (4) **ADN**: Using the primary branch and enhanced branch with the CBAM. (5) **ADN+DAMix**: Using ADN with DAMix. We train these settings on NH-Haze and test the trained models on NH-Haze and O-Haze to verify their effect on samples both within and outside the training distribution. As shown in Tab. 4, the use of the CBAM improves the performance of **PB** on $N \rightarrow N$, with performance gains of 0.58 dB in PSNR

Method	O-Haze	Dense-Haze	NH-Haze
DCP	12.92/0.505	10.06/0.386	10.57/0.520
AOD-Net	17.69/0.616	13.14/0.414	15.40/0.569
GridDehazeNet	21.91/0.730	14.10/0.513	18.01/0.657
FFA-Net	22.12/0.768	14.16/0.514	19.87/0.692
MSBDN	24.36/0.749	15.08/ <u>0.518</u>	19.23/0.706
KDDN	<u>25.45/0.780</u>	-	-
AECR-Net	-	15.80/0.466	19.88/ 0.717
ADN (Ours)	25.46/0.792	16.02/0.594	21.03/0.714

Table 3: Performance within the training distribution.

and 0.009 in SSIM. Furthermore, the CBAM achieves performance gains of 0.68 dB in PSNR and 0.01 in SSIM from **PB+EB** to **ADN**. In contrast, the dual-branch design does not improve as much as the CBAM on $N \rightarrow N$. However, the dual-branch design helps considerably more on $N \rightarrow O$. **ADN** surpasses **PB+CBAM** with PSNR/SSIM performance gain of (1.38 dB/0.008) by adding the enhanced branch. Moreover, after DAMix is applied, **ADN+DAMix** achieves PSNR/SSIM values of (21.28 dB/0.736), drastically outperforming **ADN** with (1.39 dB/0.051).

Setting	$N \rightarrow N$	$N \rightarrow O$
PB	20.07/0.700	18.65/0.666
PB+EB	20.35/0.704	19.09/0.675
PB+CBAM	20.65/0.709	18.51/0.677
ADN	21.03/0.714	19.89/0.685
ADN+DAMix	-	21.28/0.736

Table 4: Ablation study on ADN. $N \rightarrow N$ denotes trained on NH-Haze and tested on NH-Haze. $N \rightarrow O$ denotes trained on NH-Haze and tested on O-Haze.

5 Conclusion

We have introduced a novel data augmentation method named DAMix for domain adaptation on single image dehazing. DAMix has no computational overhead, yet is surprisingly effective on various learning-based methods. By applying DAMix, we can acquire unlimited hazy samples mitigating the domain discrepancy while maintaining natural appearances. Moreover, we conduct thorough experiments to verify the effectiveness and robustness of DAMix. DAMix dramatically improves the domain adaptation performance of the existing learning-based methods both quantitatively and qualitatively. Furthermore, we introduce ADN, which features a dual-branch design, a CBAM attention module, and a DAL function. We show that ADN not only achieves SOTA performance on real haze datasets but also realizes remarkable domain adaptation performance when coupled with DAMix.

References

- Ancuti, C.; Ancuti, C. O.; and Timofte, R. 2018. Ntire 2018 challenge on image dehazing: Methods and results. In *Proceedings of the IEEE Conference on Computer Vision and Pattern Recognition Workshops*, 891–901.
- Ancuti, C. O.; Ancuti, C.; Sbert, M.; and Timofte, R. 2019a. Dense-haze: A benchmark for image dehazing with dense-haze and haze-free images. In *2019 IEEE international conference on image processing (ICIP)*, 1014–1018. IEEE.
- Ancuti, C. O.; Ancuti, C.; and Timofte, R. 2020. NH-HAZE: An image dehazing benchmark with non-homogeneous hazy and haze-free images. In *Proceedings of the IEEE/CVF Conference on Computer Vision and Pattern Recognition Workshops*, 444–445.
- Ancuti, C. O.; Ancuti, C.; Timofte, R.; and De Vleeschouwer, C. 2018. O-haze: a dehazing benchmark with real hazy and haze-free outdoor images. In *Proceedings of the IEEE conference on computer vision and pattern recognition workshops*, 754–762.
- Ancuti, C. O.; Ancuti, C.; Timofte, R.; Van Gool, L.; Zhang, L.; and Yang, M.-H. 2019b. Ntire 2019 image dehazing challenge report. In *Proceedings of the IEEE/CVF Conference on Computer Vision and Pattern Recognition Workshops*, 0–0.
- Ancuti, C. O.; Ancuti, C.; Vasluianu, F.-A.; and Timofte, R. 2020. Ntire 2020 challenge on nonhomogeneous dehazing. In *Proceedings of the IEEE/CVF Conference on Computer Vision and Pattern Recognition Workshops*, 490–491.
- Berman, D.; Avidan, S.; et al. 2016. Non-local image dehazing. In *Proceedings of the IEEE conference on computer vision and pattern recognition*, 1674–1682.
- Dong, H.; Pan, J.; Xiang, L.; Hu, Z.; Zhang, X.; Wang, F.; and Yang, M.-H. 2020. Multi-scale boosted dehazing network with dense feature fusion. In *Proceedings of the IEEE/CVF Conference on Computer Vision and Pattern Recognition*, 2157–2167.
- He, K.; Sun, J.; and Tang, X. 2010. Single image haze removal using dark channel prior. *IEEE transactions on pattern analysis and machine intelligence*, 33(12): 2341–2353.
- Hong, M.; Xie, Y.; Li, C.; and Qu, Y. 2020. Distilling image dehazing with heterogeneous task imitation. In *Proceedings of the IEEE/CVF Conference on Computer Vision and Pattern Recognition*, 3462–3471.
- Huang, G.; Liu, Z.; Van Der Maaten, L.; and Weinberger, K. Q. 2017. Densely connected convolutional networks. In *Proceedings of the IEEE conference on computer vision and pattern recognition*, 4700–4708.
- Li, B.; Peng, X.; Wang, Z.; Xu, J.; and Feng, D. 2017. Aodnet: All-in-one dehazing network. In *Proceedings of the IEEE international conference on computer vision*, 4770–4778.
- Li, B.; Ren, W.; Fu, D.; Tao, D.; Feng, D.; Zeng, W.; and Wang, Z. 2018. Benchmarking single-image dehazing and beyond. *IEEE Transactions on Image Processing*, 28(1): 492–505.
- Liu, X.; Ma, Y.; Shi, Z.; and Chen, J. 2019. Griddehazenet: Attention-based multi-scale network for image dehazing. In *Proceedings of the IEEE/CVF International Conference on Computer Vision*, 7314–7323.
- McCartney, E. J. 1976. Optics of the atmosphere: scattering by molecules and particles. *New York*.
- Narasimhan, S. G.; and Nayar, S. K. 2000. Chromatic framework for vision in bad weather. In *Proceedings IEEE Conference on Computer Vision and Pattern Recognition. CVPR 2000 (Cat. No. PR00662)*, volume 1, 598–605. IEEE.
- Narasimhan, S. G.; and Nayar, S. K. 2002. Vision and the atmosphere. *International journal of computer vision*, 48(3): 233–254.
- Qin, X.; Wang, Z.; Bai, Y.; Xie, X.; and Jia, H. 2020. FFA-Net: Feature fusion attention network for single image dehazing. In *Proceedings of the AAAI Conference on Artificial Intelligence*, volume 34, 11908–11915.
- Shao, Y.; Li, L.; Ren, W.; Gao, C.; and Sang, N. 2020. Domain adaptation for image dehazing. In *Proceedings of the IEEE/CVF Conference on Computer Vision and Pattern Recognition*, 2808–2817.
- Shyam, P.; Yoon, K.-J.; and Kim, K.-S. 2021. Towards Domain Invariant Single Image Dehazing. *arXiv preprint arXiv:2101.10449*.
- Woo, S.; Park, J.; Lee, J.-Y.; and Kweon, I. S. 2018. Cbam: Convolutional block attention module. In *Proceedings of the European conference on computer vision (ECCV)*, 3–19.
- Wu, H.; Qu, Y.; Lin, S.; Zhou, J.; Qiao, R.; Zhang, Z.; Xie, Y.; and Ma, L. 2021. Contrastive Learning for Compact Single Image Dehazing. In *Proceedings of the IEEE/CVF Conference on Computer Vision and Pattern Recognition*, 10551–10560.
- Zhang, H.; Sindagi, V.; and Patel, V. M. 2018. Multi-scale single image dehazing using perceptual pyramid deep network. In *Proceedings of the IEEE conference on computer vision and pattern recognition workshops*, 902–911.
- Zhao, H.; Gallo, O.; Frosio, I.; and Kautz, J. 2016. Loss functions for image restoration with neural networks. *IEEE Transactions on computational imaging*, 3(1): 47–57.
- Zhao, H.; Shi, J.; Qi, X.; Wang, X.; and Jia, J. 2017. Pyramid scene parsing network. In *Proceedings of the IEEE conference on computer vision and pattern recognition*, 2881–2890.
- Zhu, J.-Y.; Park, T.; Isola, P.; and Efros, A. A. 2017. Unpaired Image-to-Image Translation using Cycle-Consistent Adversarial Networks. In *Computer Vision (ICCV), 2017 IEEE International Conference on*.
- Zhu, Q.; Mai, J.; and Shao, L. 2015. A fast single image haze removal algorithm using color attenuation prior. *IEEE transactions on image processing*, 24(11): 3522–3533.